Research Article | Vol. 8, No. 2 | 1 Feb 2017 | BIOMEDICAL OPTICS EXPRESS 918
Biomedical Optics EXPRESS

OCT-based full crystalline lens shape change during accommodation in vivo

EDUARDO MARTINEZ-ENRIQUEZ,* PABLO PÉREZ-MERINO, MIRIAM VELASCO-OCANA, AND SUSANA MARCOS

Instituto de Óptica "Daza de Valdés," Consejo Superior de Investigaciones Científicas, C/Serrano 121, 28006 Madrid, Spain
eduardo.martinez@io.cfmac.csic.es

Abstract: The full shape of the accommodating crystalline lens was estimated using custom three-dimensional (3-D) spectral OCT and image processing algorithms. Automatic segmentation and distortion correction were used to construct 3-D models of the lens region visible through the pupil. The lens peripheral region was estimated with a trained and validated parametric model. Nineteen young eyes were measured at 0-6 D accommodative demands in 1.5 D steps. Lens volume, surface area, diameter, and equatorial plane position were automatically quantified. Lens diameter & surface area correlated negatively and equatorial plane position positively with accommodation response. Lens volume remained constant and surface area decreased with accommodation, indicating that the lens material is incompressible and the capsular bag elastic.

OCIS codes: (110.4500) Optical coherence tomography; (110.6880) Three-dimensional image acquisition; (330.7322) Visual optics, accommodation; (100.2960) Image analysis; (330.7327) Visual optics, ophthalmic instrumentation.

References and links

1. L. F. Garner and M. K. Yap, "Changes in ocular dimensions and refraction with accommodation," Ophthalmic Physiol. Opt. **17**(1), 12–17 (1997).
2. P. Rosales, M. Dubbelman, S. Marcos, and R. van der Heijde, "Crystalline lens radii of curvature from Purkinje and Scheimpflug imaging," J. Vis. **6**(10), 1057–1067 (2006).
3. M. Dubbelman, G. L. Van der Heijde, and H. A. Weeber, "Change in shape of the aging human crystalline lens with accommodation," Vision Res. **45**(1), 117–132 (2005).
4. M. Dubbelman, G. L. Van der Heijde, H. A. Weeber, and G. F. Vrensen, "Changes in the internal structure of the human crystalline lens with age and accommodation," Vision Res. **43**(22), 2363–2375 (2003).
5. E. Gambra, S. Ortiz, P. Perez-Merino, M. Gora, M. Wojtkowski, and S. Marcos, "Static and dynamic crystalline lens accommodation evaluated using quantitative 3-D OCT," Biomed. Opt. Express **4**(9), 1595–1609 (2013).
6. P. Pérez-Merino, M. Velasco-Ocana, E. Martinez-Enriquez, and S. Marcos, "OCT-based crystalline lens topography in accommodating eyes," Biomed. Opt. Express **6**(12), 5039–5054 (2015).
7. J. E. Koretz, S. A. Strenk, L. M. Strenk, and J. L. Semmlow, "Scheimpflug and high-resolution magnetic resonance imaging of the anterior segment: a comparative study," J. Opt. Soc. Am. A **21**(3), 346–354 (2004).
8. M. Dubbelman and G. L. Van der Heijde, "The shape of the aging human lens: curvature, equivalent refractive index and the lens paradox," Vision Res. **41**(14), 1867–1877 (2001).
9. P. Rosales, M. Wendt, S. Marcos, and A. Glasser, "Changes in crystalline lens radii of curvature and lens tilt and decentration during dynamic accommodation in rhesus monkeys," J. Vis. **8**(18), 11–12 (2008) doi:10.1167/8.1.18.
10. K. Richdale, M. A. Bullimore, and K. Zadnik, "Lens thickness with age and accommodation by optical coherence tomography," Ophthalmic Physiol. Opt. **28**(5), 441–447 (2008).
11. L. Marussich, F. Manns, D. Nankivil, B. Maceo Heilman, Y. Yao, E. Arrieta-Quintero, A. Ho, R. Augusteyn, and J. M. Parel, "Measurement of Crystalline Lens Volume During Accommodation in a Lens Stretcher," Invest. Ophthalmol. Vis. Sci. **56**(8), 4239–4248 (2015).
12. E. Kim, K. Ehrmann, S. Uhlhorn, D. Borja, E. Arrieta-Quintero, and J. M. Parel, "Semiautomated analysis of optical coherence tomography crystalline lens images under simulated accommodation," J. Biomed. Opt. **16**(5), 056003 (2011).
13. A. M. Rosen, D. B. Denham, V. Fernandez, D. Borja, A. Ho, F. Manns, J. M. Parel, and R. C. Augusteyn, "In vitro dimensions and curvatures of human lenses," Vision Res. **46**(6-7), 1002–1009 (2006).
14. A. Roorda and A. Glasser, "Wave aberrations of the isolated crystalline lens," J. Vis. **4**(4), 250–261 (2003) doi:10.1167/4.4.1.

#279917 http://dx.doi.org/10.1364/BOE.8.000918
Journal © 2017 Received 2 Nov 2016; revised 15 Dec 2016; accepted 27 Dec 2016; published 18 Jan 2017

Biomedical Optics EXPRESS

15. E. A. Hermans, P. J. Pouwels, M. Dubbelman, J. P. Kuijer, R. G. van der Heijde, and R. M. Heethaar, "Constant volume of the human lens and decrease in surface area of the capsular bag during accommodation: an MRI and Scheimpflug study," Invest. Ophthalmol. Vis. Sci. **50**(1), 281–289 (2009).
16. A. L. Sheppard, C. J. Evans, K. D. Singh, J. S. Wolffsohn, M. C. Dunne, and L. N. Davies, "Three-dimensional magnetic resonance imaging of the phakic crystalline lens during accommodation," Invest. Ophthalmol. Vis. Sci. **52**(6), 3689–3697 (2011).
17. S. Kasthurirangan, E. L. Markwell, D. A. Atchison, and J. M. Pope, "MRI study of the changes in crystalline lens shape with accommodation and aging in humans," J. Vis. **11**(3), 19 (2011).
18. C. E. Jones, D. A. Atchison, and J. M. Pope, "Changes in lens dimensions and refractive index with age and accommodation," Optom. Vis. Sci. **84**(10), 990–995 (2007).
19. S. A. Strenk, J. L. Semmlow, L. M. Strenk, P. Munoz, J. Gronlund-Jacob, and J. K. DeMarco, "Age-related changes in human ciliary muscle and lens: a magnetic resonance imaging study," Invest. Ophthalmol. Vis. Sci. **40**(6), 1162–1169 (1999).
20. R. Gerometta, A. C. Zamudio, D. P. Escobar, and O. A. Candia, "Volume change of the ocular lens during accommodation," Am. J. Physiol. Cell Physiol. **293**(2), C797–C804 (2007).
21. S. A. Strenk, L. M. Strenk, J. L. Semmlow, and J. K. DeMarco, "Magnetic resonance imaging study of the effects of age and accommodation on the human lens cross-sectional area," Invest. Ophthalmol. Vis. Sci. **45**(2), 539–545 (2004).
22. S. Ortiz, D. Siedlecki, I. Grulkowski, L. Remon, D. Pascual, M. Wojtkowski, and S. Marcos, "Optical distortion correction in optical coherence tomography for quantitative ocular anterior segment by three-dimensional imaging," Opt. Express **18**(3), 2782–2796 (2010).
23. S. Ortiz, D. Siedlecki, L. Remon, and S. Marcos, "Optical coherence tomography for quantitative surface topography," Appl. Opt. **48**(35), 6708–6715 (2009).
24. S. Ortiz, D. Siedlecki, P. Pérez-Merino, N. Chia, A. de Castro, M. Szkulmowski, M. Wojtkowski, and S. Marcos, "Corneal topography from spectral optical coherence tomography (sOCT)," Biomed. Opt. Express **2**(12), 3232–3247 (2011).
25. M. Sun, P. Pérez-Merino, E. Martinez-Enriquez, M. Velasco-Ocana, and S. Marcos, "Full 3-D OCT-based pseudophakic custom computer eye model," Biomed. Opt. Express **7**(3), 1074–1088 (2016).
26. E. Martinez-Enriquez, M. Sun, M. Velasco-Ocana, J. Birkenfeld, P. Pérez-Merino, and S. Marcos, "Optical Coherence Tomography Based Estimates of Crystalline Lens Volume, Equatorial Diameter, and Plane Position," Invest. Ophthalmol. Vis. Sci. **57**(9), OCT600 (2016).
27. I. Grulkowski, M. Gora, M. Szkulmowski, I. Gorczynska, D. Szlag, S. Marcos, A. Kowalczyk, and M. Wojtkowski, "Anterior segment imaging with Spectral OCT system using a high-speed CMOS camera," Opt. Express **17**(6), 4842–4858 (2009).
28. S. Ortiz, P. Pérez-Merino, E. Gambra, A. de Castro, and S. Marcos, "In vivo human crystalline lens topography," Biomed. Opt. Express **3**(10), 2471–2488 (2012).
29. S. Ortiz, D. Siedlecki, L. Remon, and S. Marcos, "Three-dimensional ray tracing on Delaunay-based reconstructed surfaces," Appl. Opt. **48**(20), 3886–3893 (2009).
30. W. Drexler, A. Baumgartner, O. Findl, C. K. Hitzenberger, H. Sattmann, and A. F. Fercher, "Submicrometer precision biometry of the anterior segment of the human eye," Invest. Ophthalmol. Vis. Sci. **38**(7), 1304–1313 (1997).
31. S. R. Uhlhorn, D. Borja, F. Manns, and J. M. Parel, "Refractive index measurement of the isolated crystalline lens using optical coherence tomography," Vision Res. **48**(27), 2732–2738 (2008).
32. R. Navarro, L. González, and J. L. Hernández, "Optics of the average normal cornea from general and canonical representations of its surface topography," J. Opt. Soc. Am. A **23**(2), 219–232 (2006).
33. P. Rosales and S. Marcos, "Pentacam Scheimpflug quantitative imaging of the crystalline lens and intraocular lens," J. Refract. Surg. **25**(5), 421–428 (2009).
34. J. F. Koretz, C. A. Cook, and P. L. Kaufman, "Aging of the human lens: changes in lens shape at zero-diopter accommodation," J. Opt. Soc. Am. A **18**(2), 265–272 (2001).
35. O. Nishi, Y. Nishi, S. Chang, and K. Nishi, "Accommodation amplitudes after an accommodating intraocular lens refilling procedure: in vivo update," J. Cataract Refract. Surg. **40**(2), 295–305 (2014).
36. D. A. Atchison, E. L. Markwell, S. Kasthurirangan, J. M. Pope, G. Smith, and P. G. Swann, "Age-related changes in optical and biometric characteristics of emmetropic eyes," J. Vis. **8**(29), 20–21 (2008) doi:10.1167/8.4.29.
37. A. Glasser and M. C. Campbell, "Biometric, optical and physical changes in the isolated human crystalline lens with age in relation to presbyopia," Vision Res. **39**(11), 1991–2015 (1999).
38. E. A. Hermans, M. Dubbelman, G. L. van der Heijde, and R. M. Heethaar, "Change in the accommodative force on the lens of the human eye with age," Vision Res. **48**(1), 119–126 (2008).
39. E. A. Hermans, M. Dubbelman, R. Van der Heijde, and R. M. Heethaar, "Equivalent refractive index of the human lens upon accommodative response," Optom. Vis. Sci. **85**(12), 1179–1184 (2008).
40. A. de Castro, J. Birkenfeld, B. Maceo, F. Manns, E. Arrieta, J. M. Parel, and S. Marcos, "Influence of shape and gradient refractive index in the accommodative changes of spherical aberration in nonhuman primate crystalline lenses," Invest. Ophthalmol. Vis. Sci. **54**(9), 6197–6207 (2013).

Biomedical Optics EXPRESS

41. D. Siedlecki, A. de Castro, E. Gambra, S. Ortiz, D. Borja, S. Uhlhorn, F. Manns, S. Marcos, and J. M. Parel, "Distortion correction of OCT images of the crystalline lens: gradient index approach," Optom. Vis. Sci. **89**(5), E709–E718 (2012).
42. J. C. He, S. A. Burns, and S. Marcos, "Monochromatic aberrations in the accommodated human eye," Vision Res. **40**(1), 41–48 (2000).
43. E. Gambra, L. Sawides, C. Dorronsoro, and S. Marcos, "Accommodative lag and fluctuations when optical aberrations are manipulated," J. Vis. **9**(4), 1–15 (2009) doi:10.1167/9.6.4.
44. S. Plainis, H. S. Ginis, and A. Pallikaris, "The effect of ocular aberrations on steady-state errors of accommodative response," J. Vis. **5**(5), 466–477 (2005) doi:10.1167/5.5.7.
45. J. F. McClelland and K. J. Saunders, "The repeatability and validity of dynamic retinoscopy in assessing the accommodative response," Ophthalmic Physiol. Opt. **23**(3), 243–250 (2003).

1. Introduction

Understanding the changes in lens geometry with accommodation is critical to fully understand the lenticular mechanism of accommodation and for the design and evaluation of solutions for presbyopia.

Morphological changes in the lens with accommodation have been obtained in vivo using various optical imaging techniques including Purkinje [1, 2], Scheimpflug [2–4], and Optical Coherence Tomography (OCT) [5,6]. Correction of the optical distortion produced by refraction by the cornea and anterior lens surfaces is critical to obtain accurate anterior and posterior lens shape. Some controversial reports in lens radii have resulted from lack of proper corrections of these distortions [7]. In most cases the reports are based on cross-sectional images of the lens (one or two meridians), and they include changes in the lens radii of curvature and asphericity [2, 3, 8], lens tilt and decentration [9], lens internal structure [4], and dynamic phakometry [10] during accommodation. In a recent study we reported changes in lens surface elevation maps and biometry based on quantitative three-dimensional (3-D) spectral OCT [6]. Invariably all studies *in vivo* based on optical imaging analyze only the central part of the lens, visible through the pupil. While the reported changes of the lens during accommodation resulting from the ciliary muscle forces are consistent with the Helmholtz's theory of accommodation: steepening of the lens surfaces, increase in lens thickness (LT) and decrease in anterior chamber depth (ACD), estimates of other parameters not possibly measured directly with optical imaging techniques would allow a more complete experimental assessment of the theory. In particular, critical parameters include the lens volume (VOL), the lens surface area (LSA), and the diameter of the lens at the equatorial plane (DIA).

Most knowledge to date on the full shape of the accommodating lens has been obtained from *ex vivo* measurements of lenses mounted in a stretcher system that simulates accommodation, using OCT [11, 12] or, more extensively, shadow photography [13]. *Ex vivo* measurements allow visibility of the entire shape of the lens by removing cornea, iris, and the posterior pole. While in general data obtained *ex vivo* match morphological and optical parameters measured *in vivo* as a function of accommodation for equivalent accommodative stimuli (radii of curvature, power change or spherical aberration) [14], some differences between *ex vivo* and *in vivo* measurements may arise from one or more of these factors: (1) post-mortem handling and changes in the lens; (2) horizontal orientation of the lens as opposed to the up-right natural orientation of the *in vivo* lens; (3) lack of the intraocular pressure forces present *in vivo*; (4) forces in the stretcher applied only radially.

A scarce number of studies have reported *in vivo* changes of the full lens with accommodation. These studies are usually based on Magnetic Resonance Imaging (MRI) [15–17], which is able to capture non-distorted images of the entire lens. Nevertheless, the resolution is significantly lower and the acquisition times much higher than optical techniques (around 100 µm of axial pixel size and several minutes respectively, in comparison to <5 µm of axial pixel size and less than 1 second 3-D image acquisitions in typical spectral OCT). Besides, the long acquisition times and the complexity of the technique result in generally complicated experimental protocols, with the subject placed in a supine position in the MRI

Biomedical Optics EXPRESS

scanner. Furthermore, some MRI-based lens studies report data from 2-D images [18, 19], requiring therefore assumptions regarding the revolution symmetry of the lens, and limiting the accuracy in the reconstruction of several parameters such as the lens volume or surface area.

Although the accommodation-related changes in the full crystalline lens shape have been studied (*in vivo* and *ex vivo*), the mentioned assumptions and limitations have raised questions on the actual occurring changes, as the results in the literature are controversial. Several studies *in vivo* and *ex vivo* using MRI and sagittal photographs reported a change in the lens volume with accommodation [16, 20, 21], whereas studies *in vivo* using MRI and *ex vivo* using OCT with lenses mounted in a stretcher that simulates accommodation reported unchanged volume with accommodation [11, 15]. These findings have led to conflicting hypotheses: (i) the lens volume changes with accommodation due to fluid exchange between the lens and the surroundings or due to lens substance being compressible; (ii) the lens is incompressible or near-incompressible and thus the lens volume is constant with accommodation. 3-D high-resolution measurements *in vivo* of the full lens, leading to accurate estimates of full lens parameters (volume, surface, diameter and plane position) are needed to solve this question.

Anterior segment Optical Coherence Tomography combined with automatic image processing algorithms and with fan and optical distortion correction algorithms [22, 23] has proved capable of obtaining quantitative anterior segment biometry and geometry. The accuracy of the quantification capabilities of the OCT has been validated *ex vivo* with artificial model eyes with known dimensions and *in vivo* comparing with other imaging techniques (videokeratography, Scheimpflug and non-contact profilometry) [24, 25]. In addition, we have recently presented and validated a method to accurately estimate the shape of the full lens from OCT anterior and posterior lens data visible through the eye's natural pupil aperture [26]. In this method, a parametric model is proposed, which was trained and validated with *ex vivo* lenses in which the entire crystalline lens is visible. We have shown that the proposed method shows improved performance in comparison with state-of-the-art methods, leading to volume, diameter and equatorial plane position (EPP) estimation errors approximately 3, 6, and 4 times lower on average, respectively.

In the present study, we used 3-D quantitative OCT imaging and the new method for full lens shape estimation to investigate potential changes in lens volume, surface area, diameter and equatorial plane position during accommodation in 19 young eyes *in vivo*. To our knowledge, this is the first work reporting changes of the 3-D full shape of the crystalline lens during accommodation *in vivo* from OCT images.

2. Materials and methods

2.1 Subjects

Twenty-two eyes from 14 young human subjects (mean age: 28.6 ± 4.4 y.o) were studied. Three eyes from the sample were excluded after analysis because their estimated accommodative response was very low (< 2 D of accommodation response for 6 D of accommodative demand). We therefore report data on 19 eyes from 13 subjects. Refractive errors of the reported subjects ranged between −6 to + 0.75 D sphere and −1.25 to 0 D cylinder. Subjects signed a consent form approved by the Institutional Review Boards after they had been informed on the nature and possible consequences of the study, in accordance to the tenets of the Declaration of Helsinki.

2.2 OCT system

Images were acquired with a custom spectral Optical Coherence Tomography (sOCT) system based on a fiber-optics Michelson interferometer configuration with a superluminiscent diode (λ_0 = 840 nm, $\Delta\lambda$ = 50 nm) as a light source, and a spectrometer (volume diffraction grating

Biomedical Optics EXPRESS

and a 4096-pixel line-scan metal-oxide semiconductor camera) as a detector [27]. The effective acquisition speed was 25000 A-Scans/s. The axial range was 7 mm in depth, resulting in a theoretical pixel size of 3.4 µm. The nominal axial resolution (estimated from the bandwidth/coherence length of the source) was 6.9 µm in tissue.

To induce accommodation and compensate defocus, an external accommodative channel was incorporated to the OCT based on a Badal system mounted on a motorized stage (VXM-1, Velmex, Bloomfield, NY, USA) [6]. The fixation stimulus consisted of a 20/25 white Snellen E-letter presented in a black background on a Digital-Light-Processing (DLP) picoprojector (854x480 pixels, Philips NV, Amsterdam, Netherlands; 55 lum) subtending a 5-arcmin visual angle. Two neutral filters (ND 16) were placed after the picoprojector to produce an average luminance of ~30cd/m^2 in an otherwise dark environment.

2.3 Experimental protocols

Measurements were conducted after inducing mydriasis with one drop of phenylephrine, which allowed larger pupils without paralyzing the ciliary muscle and without affecting the lens geometry or topography [6]. Subject's stabilization was guaranteed by the use of a bite bar. Prior to imaging, the subject's eye pupillary axis was aligned to the optical axis of the instrument. To achieve this, the contralateral eye was covered with a patch and the subject was asked to fixate the fixation stimulus with the eye under measurement. Then, the stimulus was moved in 5 pixels-steps horizontally and vertically until the iris appeared flat in the preview OCT horizontal and vertical cross-sections, so that the OCT and pupillary axis were aligned in all measurements. The anterior segment of the eye was imaged while stimulating accommodation from 0 to 6 D, in 1.5 D steps. At least seven repeated measurements were collected in each condition. As the axial range of our sOCT system is not sufficient to capture all anterior segment surfaces in a single acquisition, three sets of 3-D images were captured sequentially at 5 seconds after blinking rapidly shifting axially the plane of focus: (i) cornea + iris, (ii) anterior lens + iris and (iii) posterior lens + iris. The second eye was measured subsequently following the same protocol.

Measurements consisted of a collection of 50 B-scans with 300 A-scans per B-scan and the scanning area was 11x11 mm. These parameters were selected to achieve a good trade-off between total acquisition time of a 3-D data set (0.6 seconds) and horizontal resolution of the surfaces. The complete measurement session for one eye of a single subject took less than 10 minutes after the pupil was dilated. Images containing artifacts (e.g., eyelids) were excluded.

2.4 OCT 3-D eye models construction

The construction of accurate 3-D eye models from OCT images consisted of three main processes: (i) automatic surfaces detection and segmentation, (ii) registration, and (iii) distortion correction.

Custom algorithms for automatic surface detection and segmentation were described in previous studies [6, 28]. The relative large data set collected in this study (more than 115000 B-scans, resulting from 22 eyes × 7 measurements/subject × 50 B-scans/measurement × 5 accommodative states × 3 foci) requires fast and robust automatic image segmentation. For this purpose, we have implemented faster and more robust algorithms compared to those of our prior publications, including improved thresholding and denoising algorithms, and parallel processing to reduce the computational time. Every B-scan is converted into a binary image that separates the areas that contain the surfaces of interest (masks) from the background. This is achieved with an improved uni-modal thresholding process that uses and adaptive threshold calculated from the statistics of the background. Then, morphological operations are applied for region filling. In the segmentation step the algorithm labels each mask (i.e., cornea, iris, anterior lens or posterior lens) using some of their properties (i.e. centroid positions or areas) and *a-priori* knowledge on the measurements (i.e. relative position or relative area of iris and cornea). Then, an AND operation between labeled masks

Biomedical Optics EXPRESS

and edges (obtained using a Canny detector) is performed in order to obtain the layers of interest. Outliers in the detected surfaces are removed by recursively fitting a low order polynomial. Further Zernike smoothing is applied in the 3-D surfaces. In this work we have also included a dedicated algorithm that improves the posterior lens detection by removing the noise that appears in the vitreous humor (behind the lens) in some subjects.

Image registration involved coordinate transformation of the images captured in the three different foci into one coordinate system. The coordinate of the pupil center was automatically detected for every focus (all containing the iris). The pupil center was taken as the origin of the coordinate system, shifting the data of every focus such that the iris appeared superimposed in all three images [6].

Fan and optical distortion correction algorithms were applied on the merged volumes for quantification by using 3-D ray tracing routines [22, 29]. The corneal group refractive index was taken as 1.385 [30], the aqueous humor group refractive index as 1.345, and the crystalline lens refractive index was obtained from the age-dependent average refractive index expression derived by Uhlhorn et al. [31].

All signal processing algorithms run automatically with no need of user interaction. The full computational processing average time per eye (one focus) was reduced from 15.83 ± 0.82 s [6] to 8.82 ± 0.60 s by including parallel processing (Intel Xeon CPU E3@3.5 GHz processor, 4 cores, 8GB RAM).

2.5 Entire lens shape estimation

A parametric model that estimates the entire lens geometry from 3-D volumes of the central part of the lens (constructed using the information visible through the pupil) was recently proposed in [26]. The model depends on two parameters that determine the shape of the full lens (i.e., for different combinations of these parameters, the obtained lens shape is different). To find the optimal parameters (and thus the model that better estimates the whole shape) they were trained and validated using cross-validation. 3-D volumes were constructed from OCT images of 27 *ex vivo* lenses, in which the information of the full lens was available. *In vivo* conditions were simulated assuming that only the information within the pupil size was available, and the estimated lens shapes using different combinations of parameters were compared to the actual lens shape to obtain the estimation error. The optimal parameters were chosen as those that minimized the estimation error. Once the parameters of the model have been found, it can be applied to *in vivo* measurements following the process outlined in Fig. 1. Lens tilt was removed before the whole shape of the lens was estimated.

2.6 Quantification

Various biometric parameters were quantified automatically from the 3-D constructed models of the anterior segment of the eye. Some of the parameters are calculated from the central part of the lens and thus can be obtained from the information within the pupil. Namely, the (1) anterior chamber depth (ACD), (2) lens thickness (LT), (3) curvature radius and asphericities of anterior (RAL, QAL) and posterior (RPL, QPL) lens surfaces, (4) lens tilt and decentration. Radius of curvature and asphericty were calculated, after 6th order Zernike approximation and tilt removal of the lens, by fitting the best sphere and conicoid [32] in a 6-mm of diameter optical zone with respect to their apexes. If 6-mm were not available in the posterior lens due to refraction of the rays in the different surfaces (i.e., beam diameter reduction) and modestly dilated pupils, all the data available were used to fit the surfaces. Lens tilt was calculated as the angle between the normal vector to the iris plane and the vector that passes through the anterior and posterior lens apexes.

Biomedical Optics EXPRESS

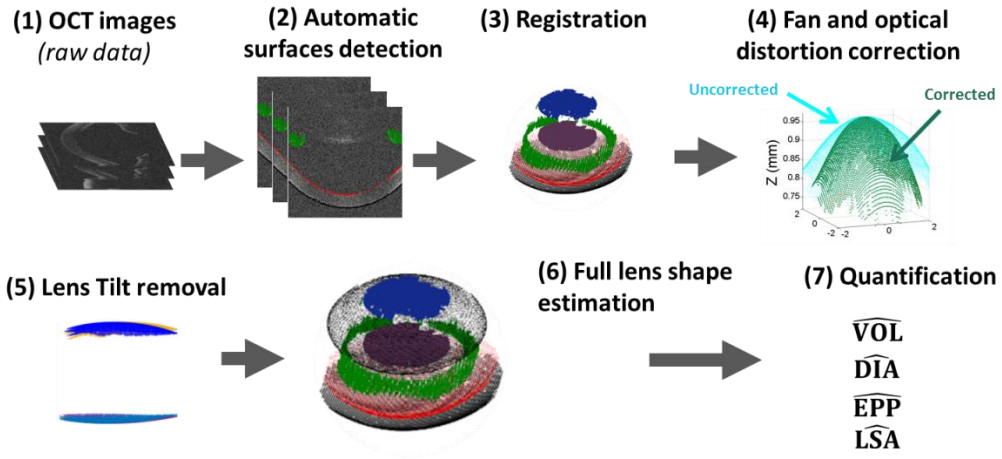

Fig. 1. Illustration of the process to quantify the 3-D anterior segment including the full shape of the lens of a specific subject from OCT images.

Parameters calculated from the whole shape of the lens included the (5) lens equatorial diameter (DIA), (6) lens equatorial plane position (EPP), (7) lens surface area (LSA), and (8) volume (VOL).

The EPP is defined as the distance from the anterior lens apex to the equatorial plane. The LSA was estimated by summing the surface area of the anterior (LSA_{ANT}) and the posterior (LSA_{POS}) parts of the lens. The surface area of the anterior/posterior lens was estimated as the sum of the triangles formed by Delaunay triangulation of the 3-D anterior/posterior lens contour in the Cartesian coordinate system. Mathematically, the area of every triangle $\mathbf{A}_i$ is calculated as:

$$\mathbf{A}_i = \frac{1}{2}\mathbf{v}_1^{(i)} \times \mathbf{v}_2^{(i)}, \tag{1}$$

where $\mathbf{v}_1^{(i)} \times \mathbf{v}_2^{(i)}$ is the cross product between any two non-parallel vectors calculated as the difference of two of the three edges that define the triangle i, and 1/2 of the modulus of the resulting vector is the area of the triangle. The $LSA_{ANT/POS}$ is then calculated as the sum of the area of the N triangles that form the Delaunay triangulation:

$$\mathbf{LSA}_{\mathbf{ANT/POS}} = \sum_{i=1}^{N} \|\mathbf{A}_i\| = \sum_{i=1}^{N} \sqrt{\mathbf{A}_i \mathbf{A}_i}. \tag{2}$$

Finally, the LSA of the full lens is given by:

$$\mathrm{LSA} = \mathrm{LSA}_{\mathrm{ANT}} + \mathrm{LSA}_{\mathrm{POS}}. \tag{3}$$

The VOL was estimated, using double integration over the region D where the lens is defined, as the sum of the VOL of the anterior and the posterior parts of the lens. Let $f_{AL}(x,y)$ and $f_{PL}(x,y)$ be the analytical functions that define the anterior and posterior lens surfaces (respectively), and $g(x,y)$ the equation of the equatorial plane of the lens. The VOL is then calculated as:

$$\mathrm{VOL} = \iint_D (f_{AL}(x,y) - g(x,y))dxdy + \iint_D -(f_{PL}(x,y) - g(x,y))dxdy. \tag{4}$$

In our study, anterior and posterior lens were the 3-D discrete surfaces of the full lens. The solution to the double integral was approximated numerically by using the trapezoidal method

Biomedical Optics EXPRESS

over *x* first and then over *y*. VOL and LSA calculations were validated using volume and surface area analytical expressions of known surfaces.

The accommodative response was estimated from the changes in the anterior segment biometry (radii, ACD and LT) with accommodation. Power of the eye was estimated using a schematic eye model in paraxial approximation as follows:

$$P_C = \frac{n_h - 1}{R_C},$$
$$P_L = (n_l - n_h)\left(\frac{1}{RAL} - \frac{1}{RPL}\right) + \frac{(n_l - n_h)^2 LT}{RAL\, n_l\, RPL}, \quad (5)$$
$$P = P_C + P_L - \frac{ACD P_C P_L}{n_h} + \frac{P_C (n_l - n_h) LT}{n_l RPL},$$

where P_C, P_L, and P are the power of the cornea, lens, and eye respectively, n_h and n_l are the refractive indexes of the aqueous humor and lens, and R_C is the anterior cornea curvature radius. For every measurement, the accommodative response was obtained comparing the average eye power focusing at far (0D) and the estimated power for the specific measurement.

2.8 Data analysis

Changes of the variables of interest (previously defined) were calculated with respect to the 0 D state (the mean value of a given variable at 0 D for each eye). The 5 measurements closer to the median for every eye and accommodation state were systematically selected from the set of measurements in order to have the same number of measurements for every accommodative state and subject. Slopes, correlation coefficients, and p-values were calculated from linear regressions between the variables of interest and accommodative response. In addition, a 2-way ANOVA analysis was conducted to further study significant dependences of the variables of interest with accommodation, subject, and interaction. Significant levels were set at $p<0.05$.

3. Results

3.1 OCT images of the anterior segment of the eye

3-D OCT images were collected in all subjects at 0-6 D (every 1.5 D step) accommodative demands. Figure 2 shows examples of raw OCT central B-scans for subject #2 for accommodative demands 0 D (left) and 6 D (middle). B-scans taken at the three different foci have been manually merged for representation purposes. Automatic registration is done in 3-D using the iris as a reference. A 3-D OCT image (consisting of 50 B-scans) for an accommodative demand of 0 D for the same subject is presented in Fig. 2 (right).

Biomedical Optics EXPRESS

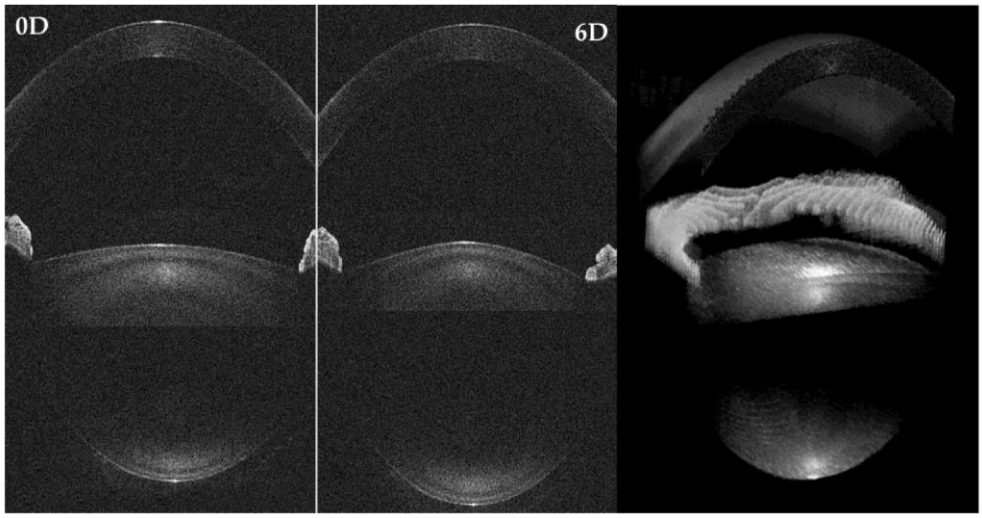

Fig. 2. Raw OCT images for subject #2: (left) 0 D of accommodative demand (Horizontal B-scan); (middle) 6 D of accommodative demand (Horizontal B-scan); (right) 3-D OCT image (consisting of 50 B-scans) at 0 D of accommodative demand.

3.2 Accommodative response

For every measurement (subject and accommodative demand state), the optical power of the eye and the lens were estimated using Eq. (5). The average eye power across subjects was 61.60 ± 2.32 D at 0 D accommodative demand. The average crystalline lens power across subjects was 17.96 ± 1.39 D and 21.93 ± 1.63 D at 0 D and 6 D accommodative demands respectively. Figure 3 shows the average accommodative response as a function of accommodative demand across subjects. The error bars represent standard deviation. On average, the change of eye power rate was 0.69 D response /D accommodative demand.

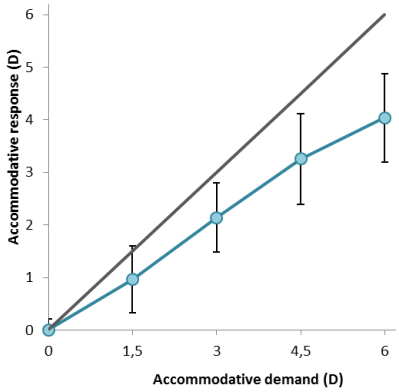

Fig. 3. Change in the optical power of the eye with accommodative demand, relative to the value obtained for the un-accommodated condition (0D). Data are average across the nineteen subjects. Error bars represent standard deviation.

3.3 Geometry of the crystalline lens at the relaxed state (0 D)

Figure 4 shows the individual geometrical parameters for each subject, for 0D accommodative demand. Data are mean values across repeated measurements and the error bars represent standard deviation. The evaluated parameters were: (A) lens volume (VOL = 147 ± 12 mm^3, on average); (B) lens equatorial plane position (EPP = 1.61 ± 0.10 mm, on

Biomedical Optics EXPRESS

average); (C) lens equatorial diameter (DIA = 8.94 ± 0.27 mm, on average); (D) lens surface area (LSA = 158 ± 8 mm^2, on average); (E) anterior chamber depth (ACD = 3.20 ± 0.21mm, on average); (F) lens thickness (LT: 3.72 ± 0.20 mm, on average); (G) radius of curvature of the anterior lens surface (RAL = 11.65 ± 1.17mm, on average); (H) radius of curvature of the posterior lens surface, in absolute value (RPL = 6.33 ± 0.48mm, on average), (I) asphericity of the anterior lens surface (QAL = –4.41 ± 3.17, on average); (J) asphericity of the posterior lens surface (QPL = –2.27 ± 1.31, on average). Subjects have been ranked by increasing VOL. VOL was statistically significantly correlated with DIA (r = 0.72; p<0.05); LSA (r = 0.88; p<<0.05); and LT (r = 0.588; p<<0.05).

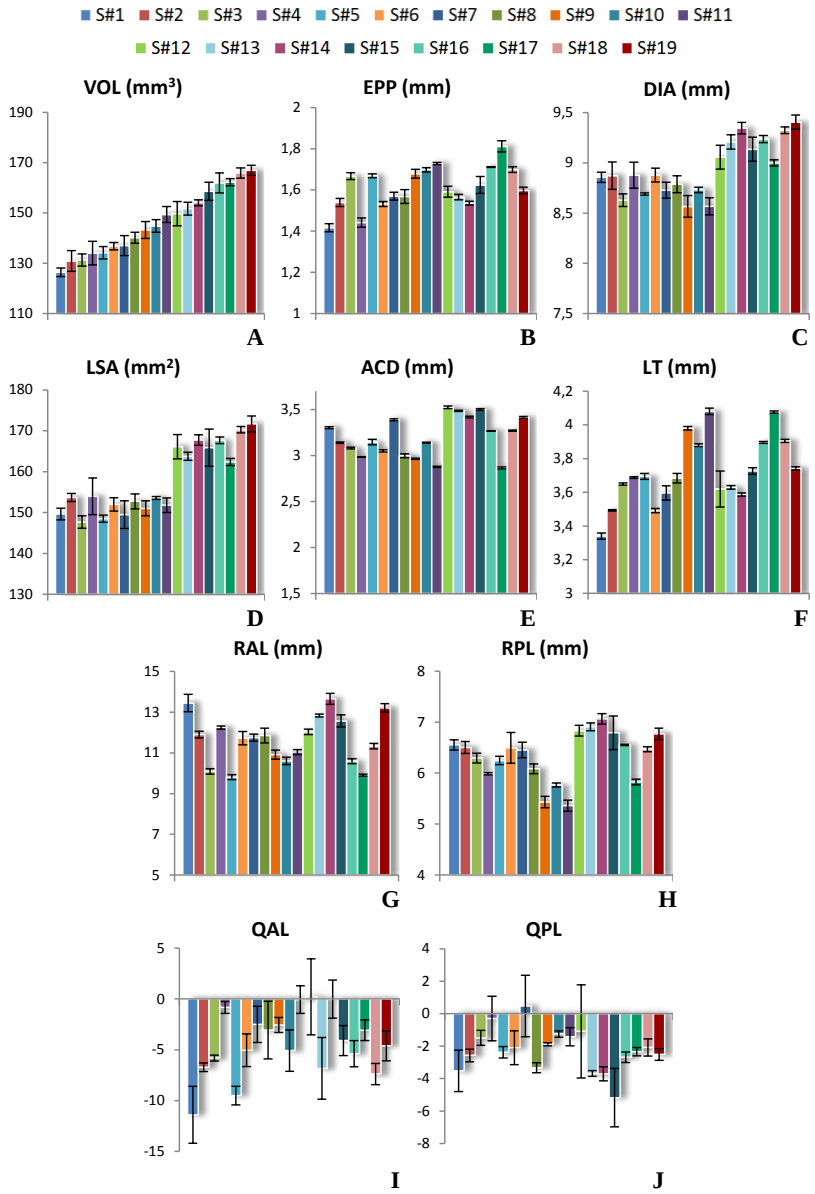

Fig. 4. Mean values and standard deviation across repeated measurements for 0 D accommodative demand for each subject: (A) VOL; (B) EPP; (C) DIA; (D) LSA; (E) ACD; (F) LT; (G) RAL; (H) RPL (in absolute value); (I) QAL; (J) QPL.

Biomedical Optics EXPRESS

3.4 Changes in anterior segment with accommodation: central part of the lens

Figure 5 shows the relative increment of: (A) RAL, (B) RPL, (C) ACD, (D) LT, (E) QAL and (F) QPL as a function of the accommodative response. For each subject, the increment is calculated with respect to the average value of the variable at 0D. Each data point represents one measurement (19 subjects × 5 measurements/subject × 4 accommodative states = 380 measurements), and each color represents a different subject. The black solid line represents the best linear fitting. RAL decreased significantly with accommodation (slope = –0.60 mm/D; r = –0.85, p<<0.05). RPL decreased (in absolute value) significantly (slope = –0.22 mm/D; r = –0.86, p<<0.5). ACD decreased significantly (slope = –0.039 mm/D; r = –0.75, p<<0.5). LT increased significantly (slope = 0.069 mm/D; r = 0.86, p<<0.5). QAL decreased significantly (slope = –0.36 D^{-1}; r = –0.16, p<<0.05). QPL increased significantly (slope = 0.30 D^{-1}; r = 0.16, p<<0.05). Lens tilt and decentration were not statistically significantly correlated with accommodative response (slope = –0.02 °/D; r = –0.0027, p = 0.89) and (slope = 0.02 mm/D; r = 0.05; p = 0.19) respectively.

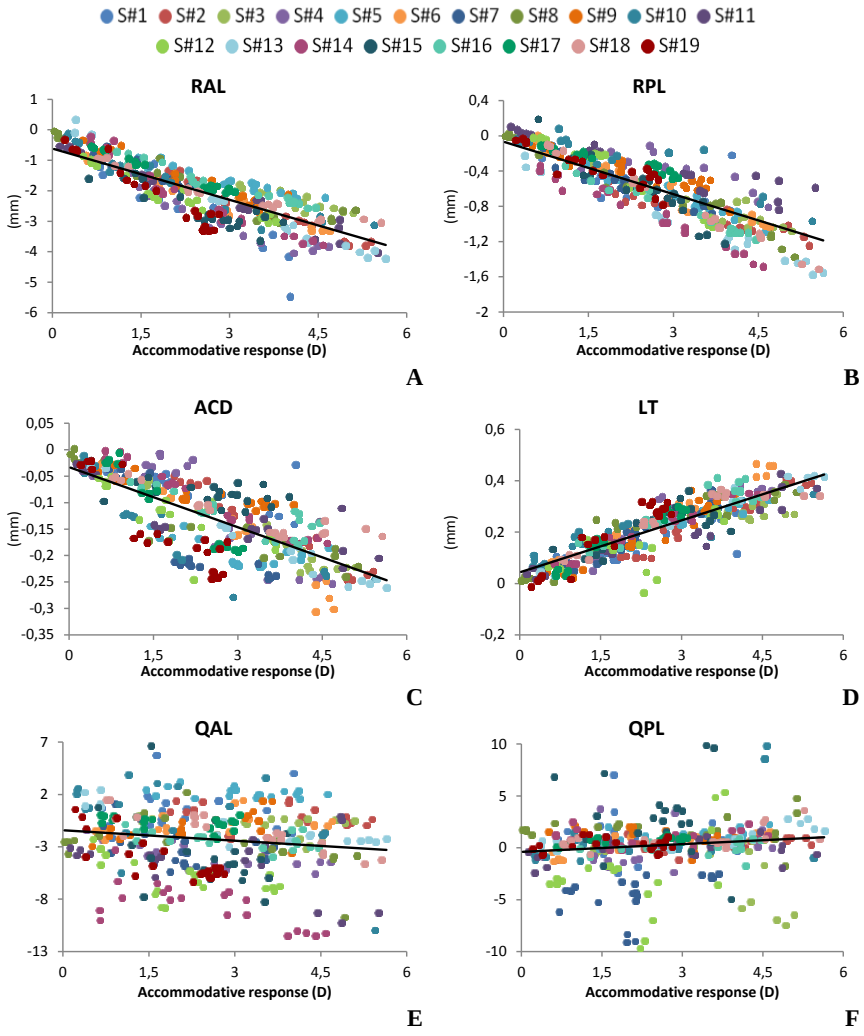

Fig. 5. Relative increment (respect to the average value of the variable at 0D) of: (A) RAL; (B) RPL; (C) ACD; (D) LT; (E) QAL; (F) QPL. Each color represents a different subject. The black solid line represents the best linear fitting.

Biomedical Optics EXPRESS

3.5 Changes in anterior segment with accommodation: full lens

Figure 6 shows the relative increment of: (A) EPP, (B) DIA, (C) LSA and (D) VOL as a function of the accommodative response. EPP increased significantly with accommodation (slope = 0.038 mm/D); r = 0.74, p<<0.05). DIA decreased significantly (slope = –0.138 mm/D; r = –0.77, p<<0.5). LSA decreased significantly (slope = –2.8 mm^2/D; r = –0.75, p<<0.5). VOL was not statistically significantly correlated with accommodative response (r = –0.09, p>0.05). A two-way ANOVA analysis showed that EPP, DIA and LSA changed significantly with accommodation and with subject. Interactions were statistically significant for EPP, DIA and LSA. The differences in lens VOL were not statistically significant with accommodation (P = 0.40).

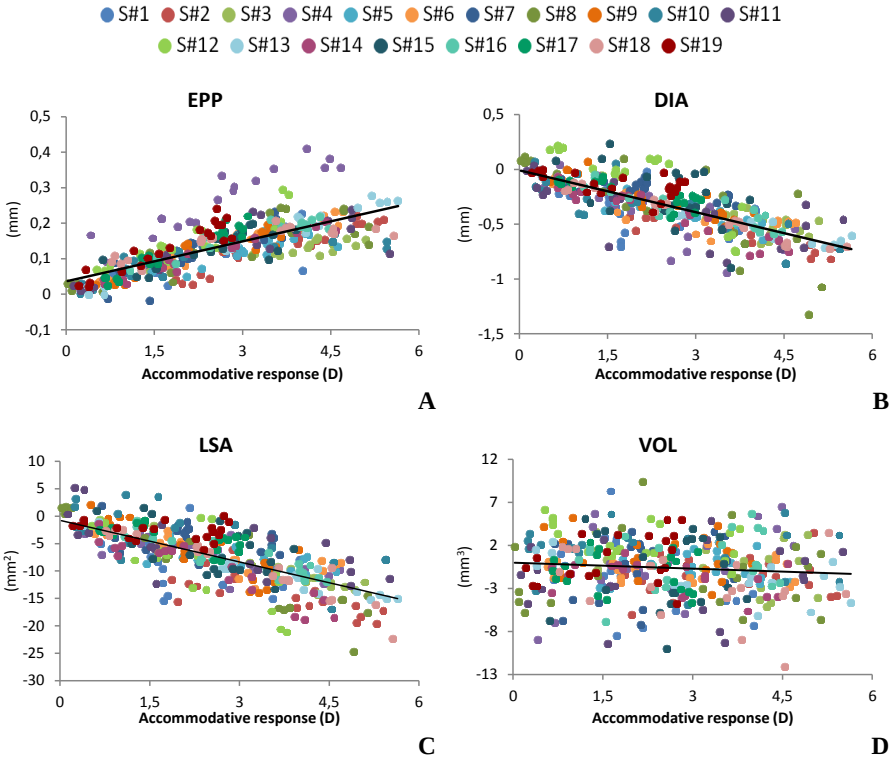

Fig. 6. Relative increment (respect to the average value of the variable at 0D) of: (A) EPP; (B) DIA; (C) LSA; (D) VOL. Each color represents a different subject. The black solid line represents the best linear fitting.

3.6 3-D models

Figure 7 shows the 3-D changes on the estimated whole lens shape with accommodation for S#2, accommodative demands 0 D (black) and 6 D (green). The iris has been removed for clarity reasons. The cornea is represented in dark green (anterior surface) and blue (posterior surface).

Biomedical Optics EXPRESS

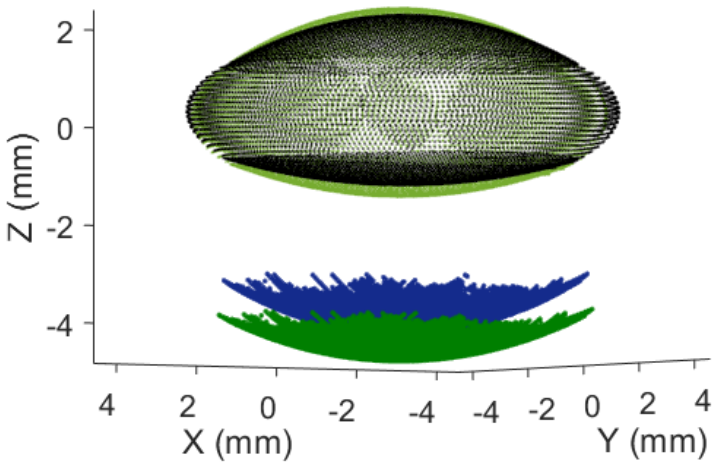

Fig. 7. 3-D changes on the estimated whole lens shape with accommodation for S#2. Accommodative demands of 0D (black) and 6D (green) are superimposed.

Note that the increase in LT is higher than the decrease in ACD (Fig. 5), and therefore the posterior surface of the lens moves backwards (although this movement is smaller in magnitude than the movement of the anterior lens towards the cornea).

4. Discussion

The high acquisition rates and resolution of OCT makes it an excellent technology for imaging *in vivo* the crystalline lens of the eye in 3-D. The study of the full crystalline lens shape changes during accommodation is crucial in the design and evaluation of solutions for presbyopia, in particular accommodating intraocular lenses or lens refilling approaches. In this paper we assessed, for the first time to our knowledge, the full lens shape as a function of accommodation *in vivo* using OCT.

Our results support the hypothesis that the lens volume is constant with accommodation and thus the lens is incompressible or near incompressible, in agreement with [11, 15]. Furthermore, the area of the lens surface decreases with accommodation, implying that the capsular bag is elastically deformed during accommodation, in agreement with [15, 16].

Advantages of OCT over other approaches

Potential changes in lens volume with accommodation have been evaluated using different imaging and surface fitting approaches and experimental conditions, which have led to controversial conclusions. Some previous studies reported an increase of lens VOL with accommodation [16, 20, 21]. As previously discussed by Marussich et al. [11], the significant increase in lens volume estimated theoretically by Gerometta et al. [20] is likely biased by the use of spherical models for the lens surfaces. Sheppard et al. [16] reported a non-significant decrease of lens volume from 0 D to 4 D and a significant increase of 2.36 ± 5.71 mm^3/D from 4 D to 8 D measured with Magnetic Resonance Imaging, which allows unobstructed viewing of the full crystalline lens *in vivo*. These results are likely affected by the measurement uncertainty intrinsic to MRI images. In general, the low resolution (800 µm × 800 µm × 800 µm voxel size in [16]) and high acquisition time (5′ 18” in [16]) in MRI can lead to inaccurate estimates of the lens geometry. Hermans et al. [15] used 3-D MRI (310 µm × 310 µm × 800 µm voxel size, 9’ 14” acquisition time) to image the complete shape of the lens, and corrected Scheimpflug imaging to validate the results obtained with MRI. The lens radii of curvature reported in that study show a high discrepancy between MRI and Scheimpflug measurements, with differences in the radius of the anterior lens ranging from 2

Biomedical Optics EXPRESS

mm to −2.4 mm, resulting in high differences in their rate of change as a function of accommodation (−1.27 mm/D with MRI and −0.63 mm/D with Scheimpflug for the same subject). Dubbelman et al. [3] reported rates of −0.61 mm/D using Scheimpflug, which are close to those we report in the current study using 3-D OCT (−0.60 mm/D), further supporting the lack of accuracy and precision of the changes estimated from MRI. We used the values of anterior and posterior lens radii and lens thickness from MRI and Scheimpflug reported by Hermans et al. in our parametric representation of the whole lens shape [26] and found that lens volume estimates from both techniques can differ more than 5%, which is in the order of magnitude of the reported changes with accommodation. This error arising from the low resolution in the MRI measurements prevents to conclude with confidence whether the volume remains constant with accommodation.

Also, there are clear advantages of using 3-D imaging compared to 2-D cross-sectional images and rotationally symmetric models to estimate lens volume [11, 18–20], as previously discussed in [11] and quantified in [26], where we concluded that errors could be up to 20 mm^3 if VOL is estimated assuming a rotationally symmetric model constructed from different cross sections.

Comparison with state of the art

There are numerous reports of the change in radii of curvature in young humans as a function of accommodation, estimated from the visible parts of the pupil. We have compared our estimates with well-established reports, as a validation of our image quantification, at least within the pupil. Our average values for RAL = 11.65 ± 1.17 mm and RPL = 6.33 ± 0.48 mm in the un-accommodated state are comparable to the values reported by Dubbleman et al. [8] (RAL = 11.24 mm and RPL = 5.9 mm) using corrected Scheimpflug imaging, for age-matched populations. Some differences may arise from the use of different fitting areas (6 mm in our study, 4 mm in [3]). Our rate of radius of curvature change per diopter of accommodation is also comparable with Dubbleman et al.'s reports: −0.61 mm/D and −0.60 mm/D for RAL, and −0.14 mm/D and −0.22 mm/D for RPL in both [3] and our study respectively. ACD/D was −0.039 mm/D in our study and −0.036 mm/D in Dubbleman et al's study and LT/D was 0.07 mm/D in both ours and Dubbleman et al's (29 year old). The rate of asphericity of the anterior lens was $-0.36\ D^{-1}$ in our study and $-0.56\ D^{-1}$ in Dubbleman et al's (6 mm fitting area in both studies), although the intersubject variability is large. Other studies using Scheimpflug imaging [33], OCT imaging [6] or MRI [18] reported data as a function of accommodative demand instead of accommodative response, making the reports less comparable.

Previous *in vivo* data of lens diameter, volume and lens surface area *in vivo* come from MRI or simple extrapolation approaches from Scheimpflug imaging [34, 35].

DIA reported in our study for un-accommodated lenses (8.94 ± 0.27 mm) is close to the one reported by Atchison et al. (9.03 ± 0.30 mm) based on MRI [36]. Nevertheless, other MRI-based data appear to overestimate DIA (e.g., 9.49 ± 0.45 mm in Sheppard et al, 9.56 ± 0.25 mm in Hermans et al.). Note that Hermans et al. estimated the diameter from different cross sections of the lens, and found discrepancies of up to 2 mm. Similar to previous reports, the equatorial diameter of the lens decrease significantly with accommodation. Our rates of changes of DIA with accommodation are higher (−0.13 mm/D) than those reported before (−0.09 mm/D in Shepard et al., −0.07 mm/D in Hermans et al.). Glasser and Campbell [37] reported correlations between the lens equatorial diameter and the lens focal length in isolated human lenses. For the range of lens focal lengths of our study, the diameter of the isolated lens ranged between 7.5 −8 mm in Glasser and Cambpell, which is consistent with the DIA of a totally accommodated lens obtained from the DIA in the un-accommodated state and the slopes estimates of our study.

Biomedical Optics EXPRESS

For VOL, our reported value for un-accommodated lenses (146 ± 12 mm^3) was lower than MRI-based data (154 ± 19 mm^3 in [16], 160.1 ± 2.5 mm^3 in [15]). In general, most optical imaging methods use an intersection approach simply extrapolating the shape of the anterior and posterior lens [13, 34, 35], which highly overestimates the lens volume (>200 mm^3). Our estimated lens surface area (LSA = 158 ± 8 mm^2) is close to the value reported by Sheppard et al. (157 ± 11 mm^2) and lower than the value reported by Hermans et al. (175 ± 2.8 mm^2). Our reported change in LSA (–2.8 mm^2/D) is higher than the values reported in previous works from MRI (–1.73 mm^2/D in [16], –1.4 mm^2/D in [15]). The strain, calculated as the change in LSA divided by the LSA at maximum accommodation, increased with accommodation, in agreement with the conclusion by [38] using a finite element model of the lens. Specifically, we obtained an average strain of 6% at 3 D and 11% at 6 D, higher than the one estimated by Hermans et al. [15] (5% at around 5 D).

It should be noted that while change in VOL with accommodation was not statistically significant, lens volume appeared to decrease with accommodation (slope = –0.22 mm^3/D), especially in some individual eyes (e.g., S#4), in agreement with Marussich et al. [11] in their *ex vivo* study, and unlike previous studies that measured an increase in lens volume with accommodation. The angle between iris and lens and the decentration changed significantly with accommodation only in some subjects.

Potential sources of error

In this study we assumed an equivalent homogeneous refractive index in the lens, which was constant with accommodation. Hermans et al. [39] did not find a significant change in the equivalent refractive index of the lens as a function of accommodation. These results were further supported by de Castro et al. [40], who estimated the lens GRIN distribution as a function of accommodation in cynomologous monkeys and found constant GRIN profile parameters with accommodation. Therefore the hypothesis of the constant index with accommodation holds.

The posterior surface of the lens in OCT *in vivo* imaging is viewed through the anterior surface, and thus is distorted by the GRIN. We assumed a homogeneous refractive index in the optical distortion correction to recover the posterior lens. The work in [11] showed that a large uncertainly in the refractive index produced an uncertainly on the order of ± 1% in the volume calculation. The study in [3] concluded that the refractive index of the lens only plays a minor part in distorting the shape of the lens, and [41] showed that the GRIN did not affect significantly the estimation of the lens radii of curvature, although the asphericity estimates may be affected. We compared the lens volumes in three *ex vivo* lenses when they were obtained measuring the lens with the anterior and posterior surfaces facing the OCT beam (after flipping the lens) and thus, not affected by the GRIN, and when the posterior lens was measured through the anterior lens and reconstructed using the equivalent refractive index of [31]. The difference in the volume estimated was around 1.5% on average.

Other potential source of error could be the estimation of accommodative response. An error in such estimation would lead to error in the slopes of the parameters as a function of accommodation. As we concluded above, using a constant refractive error with accommodation in the power estimation (Eq. (5)) should not result in a significant power estimation error. We found an accommodative response amplitude obtained from anatomical changes of 4.14 D for a 6 D accommodative demand range, similar to the accommodative response obtained in [5] using the same paraxial formula, Gambra et al., Plainis et.al, and He et al. [42–44] using Hartmann-Shack-based measurements of refraction, or McClelland and Saunders using dynamic retinoscopy and Shin- Nippon autorefractor [45]. Furthermore, we found that the slope in two well-studied parameters (ACD and LT) matched well the state of the art, which is a good indicator that the power estimation is accurate.

Robustness of the registration process had been proved previously [6], where we performed experiments removing a percentage of points of the iris (randomly taken from a

Biomedical Optics EXPRESS

uniform distribution), and we compared the estimated center point of the complete and the subsampled iris. The mean estimation error was below 2 µm for the coordinate of the center of the iris even if we removed 80% of the iris points. The repeatability of axial measurements (ACD and LT) estimated as the standard deviation across repeated measurements in the same eye was around 10 µm and 15 µm in average for the ACD and the LT respectively (Fig. 4).

Sources of error in the full shape crystalline lens estimation (lateral sampling, resolution, and extrapolation of *ex vivo*-based lens model to *in vivo* applications) were discussed in [26], where we reported a mean volume estimation error of 6.92 mm^3 when the lens was estimated from pupil sizes of 5mm. In the present study we used larger pupils (specifically, we used all the data available within the pupil) to estimate the full shape of the lens. Therefore, we can consider 6.92 mm^3 a relaxed upper bound of average estimation error, which means around a ± 2.35% of the mean lens volume.

There is an implicit variability of the crystalline lens during accommodation because of its dynamic behavior [5], which could have influence in the repeatability of the measurements. We performed at least seven measurements at every accommodative state (from which we automatically took the five closer to the median) to calculate the average and thus a more robust estimation than a single measurement. Besides, we measured at 5 different accommodative demands, as opposed to most previous works using two [15, 17, 20], thus improving the estimation of correlation values and slopes calculation. Finally, to estimate the repeatability of the measurements, we estimated the standard deviation of the five different measurements for each subject at 0 D. The repeatability, given as the mean of the standard deviations across subjects, was 2.8 mm^3 (± 0.95% of the mean lens volume). The standard deviation across all the measurements of all patients and accommodative demands was 3.25 mm^3.

In summary, distortion corrected OCT images and full shape estimation of the lens have been presented to accurately quantify the changes in the full shape of the lens with accommodation for the first time with OCT, with higher resolution and lower acquisition time than MRI. We concluded that the lens volume remains constant and that the lens surface area decreases with accommodation, indicating that the lens is incompressible and is elastically deformed during accommodation. The understanding of the accommodation process will help to improve presbyopia solutions such as accommodating IOLs or lens capsule refilling.

Funding

European Research Council under the European Union's Seventh Framework Program (FP/2007-2013) / ERC Grant Agreement (ERC-2011-AdG- 294099); Spanish Government (FIS2011-25637); Spanish Government (FIS2014-56643-R).